Frontiers of Information Technology & Electronic Engineering
www.jzus.zju.edu.cn; engineering.cae.cn; www.springerlink.com
ISSN 2095-9184 (print); ISSN 2095-9230 (online)
E-mail: jzus@zju.edu.cn

Target parameter estimation for OTFS integrated radar and communications based on sparse reconstruction preprocessing*

Zhenkai ZHANG†‡, Xiaoke SHANG, Yue XIAO

Ocean College, Jiangsu University of Science and Technology, Zhenjiang 212003, China

†E-mail: zhangzhenkai@just.edu.cn

Received July 9, 2023; Revision accepted Nov. 24, 2023; Crosschecked

Abstract: Orthogonal time-frequency space (OTFS) is a new modulation technique proposed in recent years for high Doppler wireless scenes. In order to solve the parameter estimation problem of the OTFS-integrated radar and communications system (IRCS), this paper presents the design for a parameter estimation method based on sparse reconstruction preprocessing to reduce the computational effort of the traditional weighted subspace fitting (WSF) algorithm. First, an OTFS-integrated echo signal model is constructed. Then, the echo signal is transformed to the time domain to separate the target angle from the range, and the range and angle of the detected target are coarsely estimated by using the sparse reconstruction algorithm. Finally, the WSF algorithm is used to refine the search with the coarse estimate at the center, to obtain an accurate estimate. The simulation experiments demonstrate the effectiveness and superiority of the proposed parameter estimation algorithm.

Key words: Integrated radar and communications system; Orthogonal time–frequency space; Target parameter estimation; Sparse reconstruction; Weighted subspace fitting

https://doi.org/10.1631/FITEE.2300462 **CLC number:**

unedited

1 Introduction

Radar and communication devices have been widely used in various fields (Yan et al., 2020). With the advent of the 6G era, information transmission and radar detection are facing the challenge of scarce spectrum resources, and the integrated radar and communications system (IRCS) can solve this problem by using integrated waveforms for data communication and radar detection (Dokhanchi et al., 2019; Zheng et al., 2019). IRCS can also effectively reduce the size, energy consumption, and weight of the system while increasing the spectrum utilization (Hassanien et al., 2019; Zhang et al., 2020), which makes it gradually become a hot issue for current research.

When communication waveforms are used to achieve IRCS, orthogonal frequency di-vision multiplexing (OFDM) waveforms are mainly used. Many scholars have studied the application of OFDM in radar and communication and IRCS (Sanson et al., 2020; Hakobyan and Yang, 2017; Li et al., 2019). However, OFDM-integrated signals suffer from the loss of subcarrier orthogonality in high Doppler scenarios, generating severe intercarrier interference, thus leading to the deterioration of communication and radar performance (Franken et al., 2006). To overcome this problem, orthogonal time–frequency space (OTFS) was first proposed by R. Hadani et al. (2017). Moreover, OTFS technology can be obtained by adding preprocessing and termination processing modules on top of existing multi-carrier systems (Farhang et al., 2017), which also means that OTFS can be compatible with existing OFDM systems and can be more easily deployed in B5G/6G. OTFS not

‡ Corresponding author

* Project supported by the National Natural Science Foundation of China (No. 61871203), The Postgraduate Scientific Research and Innovation Projects of Jiangsu Province (KYCX23_3878).

ORCID: Zhenkai ZHANG, https://orcid.org/0000-0003-2439-0923; Xiaoke SHANG, https://orcid.org/0009-0002-5137-2835; Yue XIAO, https://orcid.org/0009-0008-9343-5367

© Zhejiang University Press 2024

only has a high Doppler tolerance (Surabhi et al., 2019), but also enables low-latency communication with a lower peak average power than that of OFDM signals (Surabhi et al., 2019) and lower cyclic prefix (CP) requirements (Gaudio et al., 2019). In addition, OTFS has a stronger ability to eliminate multipath effects and intersymbol interference suppression (Keskin et al., 2021). Hadani et al. (2017) conducted a system-level simulation of OFDM and OTFS performance at various speeds under 4G LTE configuration, and the results showed that OTFS had a better bit error rate performance than OFDM in high-speed mobile scenarios. It was found that OTFS can achieve a performance gain of about 5 dB compared to OFDM, and the OTFS system performance is further improved with increasing subcarrier spacing.

In daily life, whether it is the connected car or intelligent internet of things (IoT) and other environments, it is particularly important for devices to realize information interaction while sensing the surrounding environment (Xue et al., 2017). In the two-dimensional plane, the position of the target can be initially determined by getting the angle and distance of the detection target (Patole et al., 2017). At present, scholars' research on OTFS technology in communication has been relatively mature, but there is less research on the application of OTFS technology to radar detection or even IRCS. In the study of Raviteja et al. (2019), OTFS was applied to the radar system for the first time, and the DD domain matching filter algorithm was proposed to detect the target speed and distance. The study proved the feasibility and effectiveness of OTFS for radar detection and showed that the OTFS radar system's speed detection accuracy was significantly better than that of the OFDM radar system. Gaudio et al. (2020) apply OTFS to IRCS and deduce the Cramer–Rao lower bound (CRLB) for OTFS signal radar target parameter estimation, and use maximum likelihood (ML) estimation to obtain parameter values in the single target case. In the study by Gaudio et al. (2020), the OTFS-integrated signal is extended to a MIMO integrated system, and the ML estimation algorithm is used to achieve multi-target radar detection and parameter estimation in the case of separable angle, delay, and Doppler domains. Inspired by the com-pressed sampling of compressed sensing, Liu et al. (2021) used prior information to cut the observation matrix to reduce computational complexity and then carried out 3D-coupled sparse Bayesian learning for parameter estimation in multi-target scenes. Li et al. (2022) proposed an integrated system based on SS-OTFS, designed the angle-of-arrival (AOA) estimation algorithm using the radar sensing matrix structure, and investigated the power allocation problem of the system. The traditional algorithms for the joint estimation of angle and delay, to achieve signal processing, mainly include the multiple signal classification (MUSIC) algorithm (Shi et al., 2019), the weighted subspace fitting (WSF) algorithm (Wang et al., 2021), the ML algorithm (Zhang et al., 2020), and the compressed sensing (CS) algorithm (Zheng and Wang, 2017; Rahman et al., 2020), etc. However, all these methods re-quire complex computational processes such as matrix decomposition, optimization, and search, and have high computational complexity.

Range and angle estimation of radar communication integrated echo signals is essential to improve radar perception of the surroundings and target localization performance. Array processing algorithms can be used for the parameter estimation of OTFS integrated systems and, in general, WSF algorithms can handle coherent signals with optimal performance (Ottersten et al., 1992). To solve the problem of the large computational effort of the WSF algorithm, this paper proposes a method based on sparse reconstruction preprocessing to reduce the computational effort. First, the sparse reconstruction algorithm uses a coarse grid to obtain coarse estimates of angles and ranges and then uses the WSF algorithm to perform accurate estimation around the coarse estimates on the search space. The received signal is dimensionally reduced in the coarse estimation to avoid the problem of information redundancy in the two-dimensional dictionary matrix, and the accurate estimation using WSF to improve the estimation accuracy. The advantage of this processing is that it enables the WSF algorithm to guarantee the parameter estimation with high accuracy, and also avoids an unnecessary grid search, which greatly reduces the computational complexity.

This paper is structured as follows: Section II constructs the received echo signal of the OTFS radar communication integration signal. In Section III, a range and angle parameter estimation algorithm based

Unedited

on sparse reconstruction preprocessing is proposed. After the simulation analysis of the proposed algorithm in Section IV, the paper is summarized in the last section.

2 Signal model

2.1 OTFS integrated transmission signal

In this paper, we consider the use of a uniform line array (ULA), which has an array element number N_a, a ULA element spacing d, and each element transmits an OTFS radar communication-integrated waveform. In order to better integrate with the existing system, the OTFS system based on OFDM is adopted in this paper (see, e.g., (Farhang et al., 2018)), at the sending end, the data symbol $x_{k,l}$, $l=0,\cdots,M-1, k=0,\cdots,\mathrm{N}-1$ is placed on the M×N two-dimensional plane, which is called the delay-Doppler plane. This plane is represented as $\Gamma=\{(k/N\Delta f, l/MT),\}$, where k is the index in the delay dimension and l is the index in the Doppler dimension. The transmitter first uses the inverse symplectic finite Fourier transform (ISFFT) to convert the $x_{k,l}$ in the delay-Doppler domain to $X_{n,m}$ in the time-frequency domain. This is given by

$$X_{n,m}=\frac{1}{\sqrt{NM}}\sum_{l=0}^{M-1}\sum_{k=0}^{N-1}x_{k,l}\exp\left(j2\pi\left(\frac{ml}{M}-\frac{nk}{N}\right)\right). \quad (1)$$

Then, a continuous time signal $s_1(t)$ is generated by the Heisenberg transform, as follows:

$$s_1(t)=\sum_{m=0}^{M-1}\sum_{n=0}^{N_c-1}X_{n,m}g_{tx}(t-mT_s)\exp\left(j2\pi n\Delta f\,(t-mT_s)\right), \quad (2)$$

where the communication data sent on the nth subcarrier of the mth OTFS symbol are denoted $X_{n,m}$. g_{tx} denotes the pulse function of the emission, T_s is the symbol period, $T_s=T_{cp}+T_u$, T_{cp} is the cyclic prefix time, and T_u is the time of the valid data on the OTFS symbol. To ensure that the individual subcarriers are orthogonal to each other, it is necessary to make $T_u=1/\Delta f$; Δf is the subcarrier frequency interval and the total frame duration is $T_f=MT_s$.

In this paper, a multi-symbol multi-pulse OTFS radar communication-integrated signal is chosen, i.e., multiple sub-pulses belonging to the same pulse are sent. The baseband signal can be obtained as:

$$\begin{aligned}s(t)=&\sum_{p=0}^{P-1}\sum_{m=0}^{M-1}\sum_{n=0}^{N_c-1}X(n,m,p)g_{tx}(t-mT_s-pT_p)\\&\exp\left(j2\pi n\Delta f\,(t-mT_s-pT_p)\right)\end{aligned}, \quad (3)$$

where T_p is the pulse repetition period, p is the number of pulses, and $X(n,m,p)$ is the communication data information represented by the nth subcarrier on the mth symbol of the pth pulse.

The baseband signal is upconverted to a transmit signal with a carrier frequency of f_c.

$$c(t)=s(t)\exp(j2\pi f_c t). \quad (4)$$

2.2 Radar receive echo signal

Assuming an observation scenario for this system where the signal transmission is line-of-sight (LOS), the reflected echo signal from K targets at a range of $R_k, k=1,2,\cdots K$. It is received at an azimuth of $\theta_k, k=1,2,\cdots,K$. Under narrowband conditions, the expression for the OTFS radar communication-integrated echo signal received by the array antenna after scattering from K targets is

$$\begin{aligned}r(t)=&\sum_{k=1}^{K}h_k\exp(-j2\pi N_a d\sin\theta_k/\lambda)s(t-\tau_k)\\&\exp\left(j2\pi f_c(t-\tau_k)\right)+n(t)\end{aligned}, \quad (5)$$

where τ_k is the delay and c is the speed of light in free space. h_k is the transmission fading factor of the k target, λ is the signal wavelength, $n(t)$ is the Gaussian white noise in the echo signal, and the carrier center frequency is f_c.

The echo signal is down-converted and the received echo signal is expressed as

$$\begin{aligned}r(t)=&\sum_{k=1}^{K}h_k\exp(-j2\pi N_a d\sin\theta_k/\lambda)\\&s(t-\tau_k)\exp(-j2\pi f_c\tau_k)+\bar{n}(t)\end{aligned}. \quad (6)$$

The echo signal is sampled and discretized, $t=iT_u/N_c+mT_s+pT_p$, and the sampling frequency is $f_s=N_c\Delta f$. The signal is narrowband and, for simplicity, the discrete signal after the constant term $\exp\left(-j2\pi f_c\frac{2R_k}{c}\right)$ is ignored as follows:

$$\begin{aligned}r_{m,p}(i)=&\sum_{k=1}^{K}\sum_{n=0}^{N_c-1}h_k X(n,m,p)\exp(-j2\pi N_a d\sin\theta_k/\lambda)\\&\exp\left(j2\pi n\Delta f\frac{iT_u}{N_c}\right)\exp\left(-j2\pi n\Delta f\frac{2R_k}{c}\right)+\bar{n}_{m,p}(i)\end{aligned}, \quad (7)$$

where $\bar{n}_{m,p}(i)=n(iT_u/N_c+mT_s+pT_p)$ is the sampling of the noise.

The echo signal received by the system, written in matrix form

$$\mathbf{R}_p=\sum_{k=1}^{K}h_k\mathbf{X}_p\mathbf{B}_k\mathbf{F}^H\mathbf{\Gamma}_k+\bar{\mathbf{N}}_p, \quad (8)$$

where $\bar{\mathbf{N}}_p$ is the matrix form of the received Gaussian white noise, $\mathbf{X}_p$ is the communication data matrix,

unedited

$$\mathbf{B}_k=\left[1,\exp\left(\frac{-j2\pi d\sin\theta_k}{\lambda}\right),\cdots,\exp\left(\frac{-j2\pi\left(N_a-1\right)d\sin\theta_k}{\lambda}\right)\right]^{\mathrm{T}}$$

represents the array guidance vector of the antenna transmitting model arriving at the receiving end, $\mathbf{F}^H$ is the Fourier transform conjugate matrix, $\mathbf{\Gamma}_k=diag(\boldsymbol{\beta}_{\mathrm{k}})$,

$$\boldsymbol{\beta}_k=\left[1,\exp\left(-j2\pi\Delta f\left(\frac{2R_{\mathrm{k}}}{c}\right)\right),\cdots,\exp\left(-j2\pi\left(N_c-1\right)\Delta f\left(\frac{2R_{\mathrm{k}}}{c}\right)\right)\right]^T$$

, and $\boldsymbol{\beta}_k$ is the delay vector.

For the radar communication-integrated signal, the communication information carried in the echo signal will affect the detection performance of the system. For radar, the communication information carried by the echo signal can be known if the transmitted waveform is known, that is, the communication data $X\left(n,m,p\right)$ of the OTFS integrated signal. In order to eliminate the impact of communication information on detection performance and achieve more accurate estimation, the communication information in the received data can be compensated directly before radar signal processing. First, the received echo signal is multiplied with the discrete Fourier transform matrix $\mathbf{F}^{-1}$ to change the signal to the frequency domain, and then the inverse matrix of the information matrix $\mathbf{X}_p^{-1}$ is used to compensate the communication information of equation (8):

$$\mathbf{F}^{-1}\mathbf{R}_p\mathbf{X}_p^{-1}=\sum_{k=1}^{K}h_k\mathbf{B}_k\mathbf{\Gamma}_k+\mathbf{F}^{-1}\bar{\mathbf{N}}_p\mathbf{X}_p^{-1}. \tag{9}$$

Define the expressions for the pth received pulse matrix and the noise matrix after pre-processing as $\tilde{\mathbf{R}}_p=\mathbf{F}\mathbf{R}_p\mathbf{X}_p^{-1}$ and $\tilde{\mathbf{N}}_p=\mathbf{F}\bar{\mathbf{N}}_p\mathbf{X}_p^{-1}$.

The received matrices are combined by column and, after information compensation and rearrangement, the matrix contains only the angle and range information of the radar detection target to be estimated. Define the receive model expression as

$$\tilde{\mathbf{R}}=\tilde{\mathbf{A}}\tilde{\mathbf{H}}+\tilde{\mathbf{N}}, \tag{10}$$

where

$$\tilde{\mathbf{A}}=[\tilde{\mathbf{a}}\left(R_1,\theta_1\right),\tilde{\mathbf{a}}\left(R_2,\theta_2\right),\cdots,\tilde{\mathbf{a}}\left(R_k,\theta_k\right)] \tag{11}$$

$$\tilde{\mathbf{a}}\left(R_k,\theta_k\right)=\boldsymbol{\theta}_k\otimes\boldsymbol{\beta}_k \tag{12}$$

$$\tilde{\mathbf{H}}=[1,h_1,\cdots h_k]^{\mathrm{T}} \tag{13}$$

$$\boldsymbol{\beta}_k=\left[1,\exp\left(-j2\pi\Delta f\left(\frac{2R_{\mathrm{k}}}{c}\right)\right),\cdots,\exp\left(-j2\pi\left(N_c-1\right)\Delta f\left(\frac{2R_{\mathrm{k}}}{c}\right)\right)\right]^T \tag{14}$$

$$\boldsymbol{\theta}_k=\left[1,\exp\left(\frac{-j2\pi d\sin\theta_k}{\lambda}\right),\cdots,\exp\left(\frac{-j2\pi\left(N_a-1\right)d\sin\theta_k}{\lambda}\right)\right]^{\mathrm{T}}. \tag{15}$$

The parameter matrix containing the angles and ranges is expressed as

$$\mathbf{\Phi}=\begin{bmatrix}\mathbf{\Phi}_1\\ \mathbf{\Phi}_2\\ \vdots\\ \mathbf{\Phi}_{N_{\mathrm{a}}}\end{bmatrix}=\tilde{\mathbf{A}}\tilde{\mathbf{H}}. \tag{16}$$

3 OTFS integrated target parameter estimation based on sparse reconstruction pre-processing

3.1 WSF algorithm

The WSF algorithm is considered to be one of the most commonly applied and reliable parameter estimation algorithms in array signal processing, and it is known from the parameter selection criterion of the WSF algorithm that the algorithm can handle signals with correlation. The specific algorithm proof and derivation can be found in the study by Ottersten et al. (1993).

To get the angle and range data of the detection target, the covariance matrix of the received narrowband signal vector in (10) needs to be found as

$$\mathbf{R}_{\tilde{R}}=\frac{1}{M}\tilde{\mathbf{R}}\tilde{\mathbf{R}}^H. \tag{17}$$

Eigenvalue decomposition of the resulting covariance matrix,

$$\mathbf{R}_{\tilde{R}}=\mathbf{U}_{\tilde{R}}\mathbf{\Sigma}_{\tilde{R}}\mathbf{U}_{\tilde{R}}^{\ H}=\mathbf{U}_S\mathbf{\Sigma}_S\mathbf{U}_S^{\ H}+\mathbf{U}_N\mathbf{\Sigma}_N\mathbf{U}_N^{\ H}, \tag{18}$$

where $\mathbf{U}_{\tilde{R}}$ and $\mathbf{U}_N$ are the eigenvectors corresponding to the signal subspace and noise subspace, respectively, and $\mathbf{\Sigma}_{\tilde{R}}$ and $\mathbf{\Sigma}_N$ are the eigenvalue diagonal matrices.

In the ideal case, the eigenvalues after covariance eigendecomposition are mutually orthogonal and linearly independent; the signal subspace is a linear subspace of the array manifold tensor $span\left\{\mathbf{U}_S\right\}=span\left\{\tilde{\mathbf{A}}\right\}$, and there exists a full rank matrix such that

$$\mathbf{U}_S=\tilde{\mathbf{A}}\mathbf{T} \tag{19}$$

$$\mathbf{T}=\mathbf{R}_S\mathbf{A}^H\mathbf{U}_S\left(\mathbf{\Sigma}_S-\sigma^2\mathbf{I}\right)^{-1}. \tag{20}$$

The problem of spatial mismatch arises when there is noise interference in the signal, so the WSF is used to construct a fitting relationship with which to obtain a matrix that allows (19) to hold, and to ensure that the two spaces fit best under least squares,

$$\theta,\hat{\mathbf{T}}=\min\left\|\mathbf{U}_S-\tilde{\mathbf{A}}\hat{\mathbf{T}}\right\|_F^{\ 2}. \tag{21}$$

In the above equation, $\theta=[\mathrm{R}_1,\cdots,\mathrm{R}_K,\theta_1,\cdots,\theta_K]^{\mathrm{T}}$ represents the range and angle parameters of the detection target to be estimated and $\hat{\mathbf{T}}$ is an auxiliary parameter. Therefore, by fixing the value of $\tilde{\mathbf{A}}$, we can obtain a

unedited

solution that fits the least squares fit as

错误!不能通过编辑域代码创建对象。. (22)

Substituting the least squares fit solution (22) for $\hat{\mathbf{T}}$ into equation (21) yields

$$\begin{aligned}\theta &= \min\left\|\mathbf{U}_S - \mathbf{A}\mathbf{A}^{+}\mathbf{U}_S\right\|_F^2 \\ &= \min tr\left\{\mathbf{P}_A^{\perp}\mathbf{U}_S\mathbf{U}_S^{H}\right\} = \max tr\left\{\mathbf{P}_A\mathbf{U}_S\mathbf{U}_S^{H}\right\}\end{aligned}. \quad (23)$$

It is evident that the answer to the signal subspace fit is the optimization issue of (22), and a generalization of equation (21) yields the fitting problem using the matrix W to weight the signal subspace, which can be written as

$$\theta, \hat{\mathbf{T}} = \min\left\|\mathbf{U}_S\mathbf{W}^{\frac{1}{2}} - \tilde{\mathbf{A}}\hat{\mathbf{T}}\right\|_F^2. \quad (24)$$

The solution for the estimated detection target parameters can be obtained as

$$\theta = \min tr\left\{\mathbf{P}_A^{\perp}\mathbf{U}_S\mathbf{W}\mathbf{U}_S^{H}\right\} = \max tr\left\{\mathbf{P}_A\mathbf{U}_S\mathbf{W}\mathbf{U}_S^{H}\right\} \quad (25)$$

when the signal subspace weighting matrix satisfies

$$\mathbf{W}_{Sopt} = \left(\mathbf{\Sigma}_S - \sigma^2\mathbf{I}\right)^2\mathbf{\Sigma}_S^{-1}. \quad (26)$$

The resultant values of the parameter estimation of the weighted subspace fitting algorithm for the optimal weights can be obtained by solving equation (25). In this paper, to further reduce the difficulty of solving this multidimensional optimal problem, an alternate projection (AP) transform is used to convert the complex multidimensional optimal search into multiple simple one-dimensional solved optima. In this solution process, the expression for the kth detection target at the moment of the $i+1th$ iteration,

$$\left(\hat{R}_k^{\,i+1}, \theta_k^{\,i+1}\right) = \max tr\left\{\mathbf{P}_{\tilde{A}_k^{\,i}}\mathbf{U}_S\mathbf{W}_{Sopt}\mathbf{U}_S^{H}\right\}, \quad (27)$$

where $\tilde{A}_k^{\,i} = \left[\tilde{A}_1^{\,i}, \tilde{A}_2^{\,i} \cdots \tilde{A}_k\right]$ represents a matrix where column $k-1$ contains previously computed parameter vectors, and column k contains corresponding vectors for the target parameters currently under estimation. The algorithm iterates for a total of K cycles to estimate the target parameters.

3.2 Pre-processing based on sparse reconstruction

The WSF algorithm of equation (25) requires a global search over range and angle, as K cycles of $NN_aN_1N_{a1}$ iterations are required in the search process; where the array stream length is NN_a, N_1 is the number of subgrids searched for range, and N_{a_1} is the number of subgrids searched for angle, the search scope and complexity are too large. A sparse reconstruction method with good parameter estimation performance and resolution is presented below as a way to narrow the search and reduce the computational effort. According to the idea of sparse reconstruction, the two-dimensional spatial plane of the radar detection target is considered in the ordinary OTFS narrowband array signal model, and the detection range of range and angle is divided into ts and rs grid points, respectively. Let the set $[\tilde{\theta}_1, \tilde{\theta}_2, \cdots, \tilde{\theta}_{ts}]$ and the set $\left[\tilde{r}_1, \tilde{r}_2, \cdots, \tilde{r}_{rs}\right]$ contain angle and range information that can cover all possible positions of the detection target, of which there are only K real existing target points, which is much smaller than the number of divided grids, so we can regard the range and angle spectrum as sparse. To address the problem that the two-dimensional grid division in the sparse representation model of the received signal increases the difficulty of signal reconstruction, this paper converts the two-dimensional reconstruction into one-dimensional reconstruction to reduce the complexity of the algorithm.

For equation (16), the elements of row n_a of the parameter matrix $\mathbf{\Phi}$ are written as

$$\mathbf{\Phi}_{n_a} = \begin{bmatrix} \sum_{k=1}^{K} h_k \exp\left(-j2\pi n_a d \sin\theta_k / \lambda\right) \\ \vdots \\ \sum_{k=1}^{K} h_k \exp\left(-j2\pi n_a d \sin\theta_k / \lambda\right)\exp\left(-j2\pi\left(N_c - 1\right)\Delta f\left(\frac{2R_k}{c}\right)\right) \end{bmatrix}^T \quad (28)$$

Each element of the row vector contains information about the parameters of the detection target, the same phase caused by the detection angle and a fixed phase difference generated by the detection range, and a Fourier transform of equation (28) converts the data to the time domain

$$\begin{aligned}X_{row}(l) = \frac{1}{N}\sum_{k=1}^{K} h_k \exp\left(-j2\pi\left(N_c - 1\right)\Delta f\left(\frac{2R_k}{c}\right)\right) \\ \sum_{n=0}^{N-1}\exp\left(j2\pi n\left(\frac{l}{N} - \Delta f\left(\frac{2R_k}{c}\right)\right)\right)\end{aligned}. \quad (29)$$

According to the above equation, it can be seen that the magnitude of the time domain data vector X_{row} can be taken to its maximum value when the index is $l_{\max} = N\Delta f\tau$. Substituting the index at the maximum value into equation (29), we can get

$$X_{row}\left(l_{\max}\right) = \sum_{k=1}^{K} h_k \Delta \exp\left(-j2\pi n_a d \sin\theta_k / \lambda\right), \quad (30)$$

where Δ is the error term, and $\Delta = \frac{1}{N}\sum_{n=0}^{N-1}\exp\left(j2\pi n\left(\delta / N\right)\right)$, $0 < \delta < 1$; that is, when the row vector takes the maximum value, the phase change information caused by the delay has been eliminated and only the target angle information remains in the parameter information matrix. After the

unedited

above analysis, the inverse Fourier transform can be performed in equation (16) by row, and the data with the largest magnitude in the transformed matrix will be presented and written as

$$\mathbf{X}_{\max} = \mathbf{A}\begin{bmatrix} \zeta_1 \\ \vdots \\ \zeta_K \end{bmatrix}, \tag{31}$$

where $\zeta_i = h_i\Delta, i = 1,\cdots,K.$, and the separation of the range and angle parameters of the detection target is completed. A two-dimensional to one-dimensional downscaling of equation (31) is performed to expand the guide vector

$$\mathbf{X}_{\max} = \tilde{\mathbf{A}}\zeta, \tag{32}$$

where $\tilde{\mathbf{A}}$ is a redundant dictionary matrix and ζ contains K non-zero elements, which only appear when the angle is the true angle of the detection target, with each non-zero element corresponding to a target parameter.

For equation (32), the l_1 parametric constraint function is constructed in order to obtain information on the angle parameters of the detection target

$$\begin{cases} \min\|\zeta\|_1 \\ s.t.\|\mathbf{X}_{\max} - \tilde{\mathbf{A}}\zeta\|_2 < \varepsilon \end{cases}. \tag{33}$$

Equation (33) can be solved directly using the CVX software package. The angle corresponding to the column vector in $\tilde{\mathbf{A}}$, corresponding to the non-zero element in ζ , is the coarse estimate of the angle, i.e., $\{\tilde{\theta}_1,\cdots,\tilde{\theta}_K\}$, and the coarse estimate of the detection target range $\hat{R} = i_{\max}c_0 / N\Delta f$ can be obtained from the peak index.

3.3 Accurate estimation of OTFS integration target parameters

At this point, initial estimates of the angle and range of the OTFS integration target have been obtained. In the sparse reconstruction method, although the discrete Fourier transform is used to separate the angle and range information in the received signal of the array, the two-dimensional dictionary matrix is reduced to a one-dimensional dictionary matrix, and the complexity of the algorithm is reduced. However, the limitations of the discrete Fourier operation make the estimation accuracy low, and only the rough spectral peak positions of the detection target parameters can be obtained. The WSF algorithm uses this coarse estimate as the center for determining the search range, and the new search space range is further improved by a more refined subgrid division, with the updated search space range and angle subgrids being N_2 and N_{a_2} . Since the coarse estimate of the sparse reconstruction algorithm reduces the global search range of angles and ranges to a single region, the WSF reduces unnecessary search steps, resulting in a significant reduction in the number of iterations. The steps of the integrated target parameter estimation algorithm based on sparse reconstruction preprocessing are as follows:

Algorithm 1: Integrated target parameter estimation algorithm based on sparse reconstruction preprocessing

1. Inverse Fourier transform of the parameter matrix $\mathbf{\Phi}$ to obtain time domain data.
2. Put forward the data with the largest amplitude in the time-domain data matrix and write it in matrix form.
3. Construction of the l_1 -parametric constraint function (33).
4. Solved using the CVX toolkit to obtain a coarse estimate of the angle.
5. Use $\hat{R} = i_{\max}c_0 / N\Delta f$ to find a rough estimate of the range.
6. Update the parameter fine estimate search space based on the coarse estimate of the detection target parameters obtained in step 5.
7. Calculate the covariance matrix $\mathbf{R}_{\tilde{R}}$, in (17).
8. Eigenvalue decomposition and ordering, construction of signal subspace $\mathbf{U}_S$, in (19).
9. Compute the optimal value of the weighting matrix $\mathbf{W}_{Sopt}$ using (26).
10. Initialization parameters $k = 1$, $i = 1$.
11. Update the search space for detecting the angle and range parameters of the target.
12. Update the matrix.
13. Calculate and record the results.
14. $i = i + 1$.
15. Until $i = N_2 N_{a_2}$.
16. The location of the spectral peak is found, i.e., the parameters θ_k , R_k .
17. $k = k + 1$.
18. Until $k = K$.

4 Computer simulation analysis

In this section, the effectiveness of the proposed algorithm is simulated. Different methods and different metrics are applied to the simulations, and the superiority of the proposed algorithm is demonstrated with regard to estimation error, theoretical error, and resolution in several ways. Considering the exact estimation in the MUSIC algorithm, the WSF algo-

unedited

rithm, and the proposed algorithm, there is a process of angle and range grid search and the estimation accuracy is related to the search grid density. This section sets the number of subgrids for angle and range division to $N_1 = N_{a_1} = 16$, where the subgrids are expanded by one adjacent grid in the algorithm proposed in this paper, as well as further subdivision with a fine fraction of 2. Information on the OTFS radar communication integration parameters used for the simulation is set up with reference to the study by Gaudio et al. (2020) and Raviteja et al. (2018), as shown in Table 1.

Table 1 System parameters.

Parameters	Symbols	Value
Carrier frequency	f_c	5.9GHz
OTFS symbols	M	8
Signal bandwidth	B	10MHz
Subcarriers	N_c	16
Number of array elements	N_a	16
Number of pulses	P	16
Symbol duration	T_u	1.6us
Cyclic prefix time	T_{cp}	0.2us
Complete symbol period	T_s	1.8us
Pulse repetition period	T_p	100us

4.1 Parameter estimation accuracy and computing time as influenced by SNR

The parameter estimation performance of the proposed algorithm, the ESPRIT algorithm, the MUSIC algorithm, and the conventional WSF algorithm with different signal-to-noise ratios (SNR) is given in Figure 1. The communication information is generated randomly and 16QAM is used to generate the communication modulation information. The other simulation parameter information is the same as in Table 1, and the radar detection target is set to be a single target at a range and angle of 1020m and 60°.

From Figure 1, we can see that the algorithm in this paper has more efficient estimation results compared to other algorithms for SNR, and has a higher estimation accuracy with fewer errors even at a small SNR.

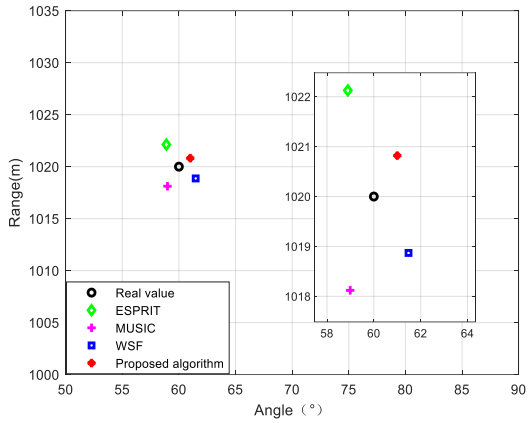

(a)

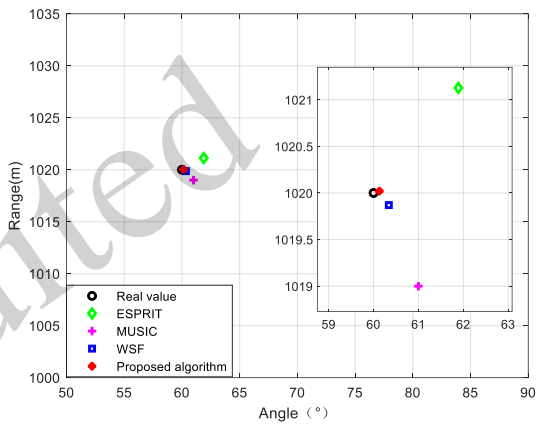

(b)

Fig.1 Parameter estimation performance at different SNRs, Comparison of the target parameter estimation results for SNR=-5dB (a), Comparison of the target parameter estimation results for SNR=5dB (b)

Next, the accuracy of the parameter estimation between the algorithm in this paper and the comparison algorithm is further investigated. To obtain the root mean square error (RMSE) shown in Figure 2, the incremental step of SNR was selected as 5 dB, which incremented the SNR from -20 dB to 5 dB. The angle and range parameters for the three targets were set to (-45°, 900 m), (60°, 1040 m), and (80°, 1080 m), respectively; the other parameters were the same as those presented in Table 1, and the number of Monte Carlo experiments was set to 100. Figure 2 reflects the parameter estimation errors for angle and range.

unedited

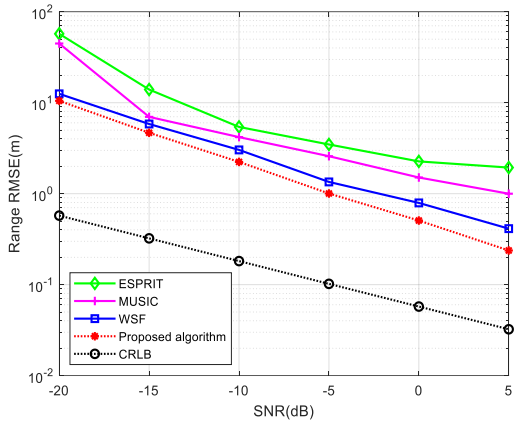

(a)

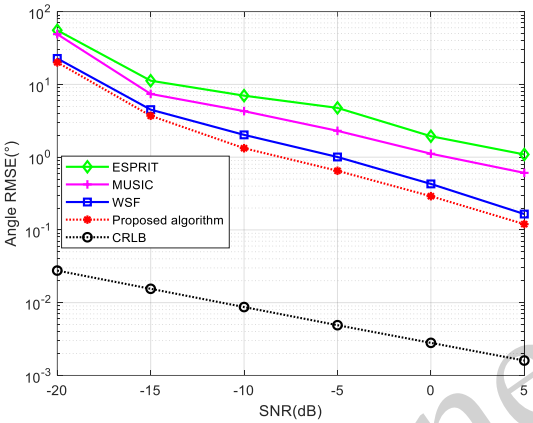

(b)

Fig. 2. Multi-target estimation performance versus SNR. Range estimated RMSE versus SNR transformation curve (a). Angle estimation RMSE versus SNR transformation curve (b).

The simulation results shown in Figure 2 further reflect the advantage of this paper's algorithm over the ESPRIT algorithm, MUSIC algorithm, and traditional WSF algorithm in terms of estimation accuracy. Although the estimation quality of all algorithms is improving with increasing SNR, the estimation performance of this paper's algorithm is more effective than that of the other algorithms and is closer to the CRLB. The worst estimation performance of the ESPRIT algorithm is because this algorithm requires a certain phase difference between the received signals, and the phase difference cannot exceed a certain range; otherwise, it will lead to errors in the angle estimation. The MUSIC algorithm outperforms the ESPRIT algorithm because it uses the orthogonality of the array vector to the noise subspace to search for the spectral peaks of angle and range. Since WSF performs the fitting of the signal subspace, it has a higher estimation accuracy. However, since our proposed algorithm uses coarse estimation to obtain a more accurate search region and performs further subdivision of the sub-subgrid, its estimation accuracy is higher than that of the WSF algorithm and it performs optimally.

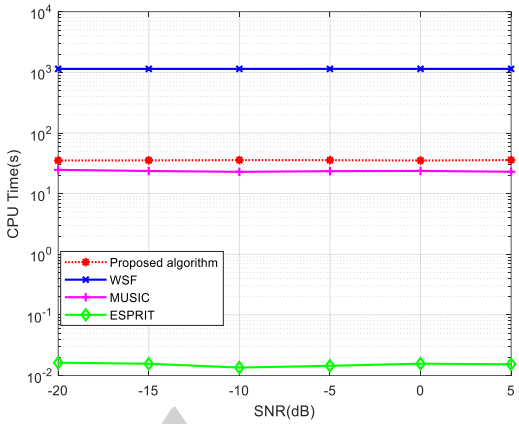

Fig. 3. Operation time.

In terms of the operation time, as shown in Figure 3, the ESPRIT algorithm is numerical and therefore has the lowest operation time, but it has the largest estimation error. The MUSIC algorithm requires a grid peak search of the spatial spectral function and therefore has a larger operation time than ESPRIT. The conventional WSF algorithm performs a large number of iterative searches to maintain the estimation accuracy, thus resulting in the longest computing time. However, the running time of the proposed algorithm is less than that of the traditional WSF algorithm because of the lower computational complexity of the reduced dimensional sparse reconstruction algorithm, and the coarse estimate greatly reduces the unnecessary search intervals in the WSF algorithm, thus decreasing the number of iterations of the search and reducing the computation time of the proposed algorithm while maintaining the same estimation reliability.

4.2 Performance comparison with different subcarrier numbers and array elements

In this subsection, the influence of the number of array elements and the number of subcarriers on the proposed algorithm and the comparison algorithm is analyzed. The number of array elements is fixed at 16, the number of subcarriers is taken as [4 8 16 32 64], and the other parameters remain the same as those in the simulation described in Section 4.1. The simulation yields the curves of the variation of the range and angle estimation performance of the detection target with the SNR (Figure 4). It can be seen that the estimation accuracy of the algorithm is improved with the

unedited

increase of subcarriers; overall, the proposed algorithm has the best estimation accuracy, and the quantity of subcarriers has more of an effect on the range estimation accuracy.

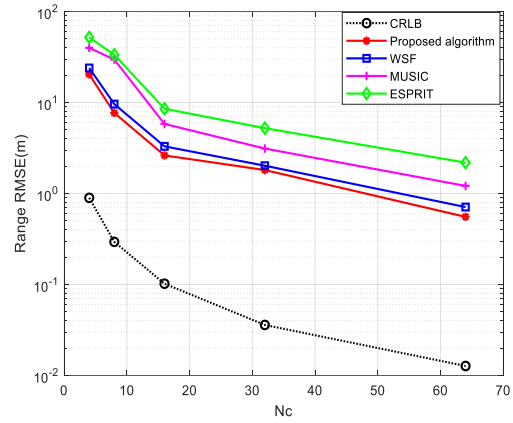

(a)

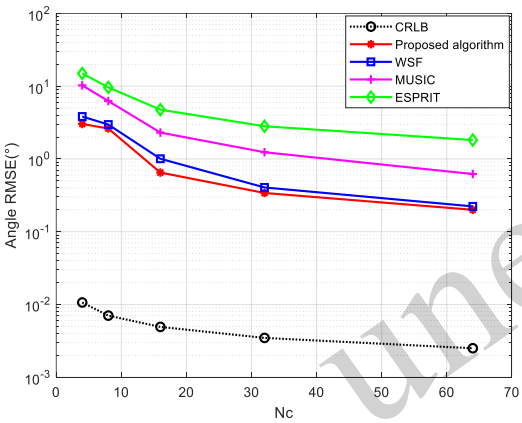

(b)

Fig. 4. Multi-target estimation performance versus number of subcarriers N_c. Range estimation RMSE versus N_c transformation curve (a). Angle estimation RMSE versus N_c transformation curve (b).

To investigate the influence of the number of arrays on the estimation performance of the method, the number of subcarriers is set to 16, the number of arrays is set to [4 8 16 32 64], and the other parameters remain unchanged from the previous section. According to the simulation results presented in Figure 5, the more antenna arrays of the OTFS radar communication integrated system there are, the better the algorithm's parameter estimation performance will be, and the proposed algorithm has the best angle and range parameter estimation performance. The proposed algorithm has the best performance in estimating the angle and range parameters, and the number of array elements has a greater influence on angle estimation accuracy.

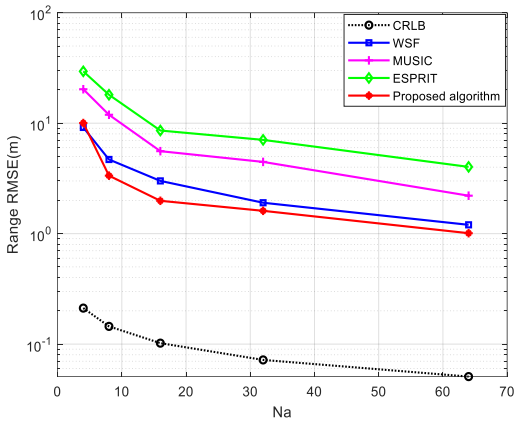

(a)

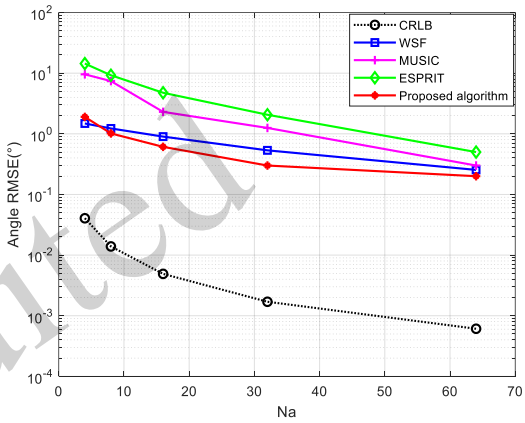

(b)

Fig. 5. Multi- target estimation performance versus number of array elements. Range estimation RMSE versus N_a transformation curve (a). Angle estimation RMSE versus N_a transformation curve (b).

4.3 Resolution performance

In order to analyze and verify the resolution of the proposed algorithm for detecting targets, two target points with the same range and similar angles are selected in this section to analyze the angle resolution of the algorithm. In the angle resolution simulation experiments, two target points are selected with a range of 1020m and angles of 40° and 43°, respectively. Two more target points with the same angle and a similar range are selected to analyze the range resolution of the algorithm. In the range resolution experiments, the two target points were selected with an angle of 40° and a range of 1020m and 1023m, respectively, and the echo SNR of the target was chosen to be SNR=10dB. In order to improve the resolution, the number of subcarriers and array elements was set to 32, and other simulation parameters were the same as those in Section 4.1.

unedited

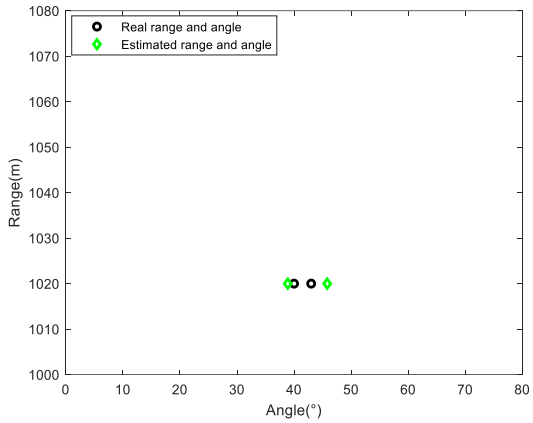

(a)

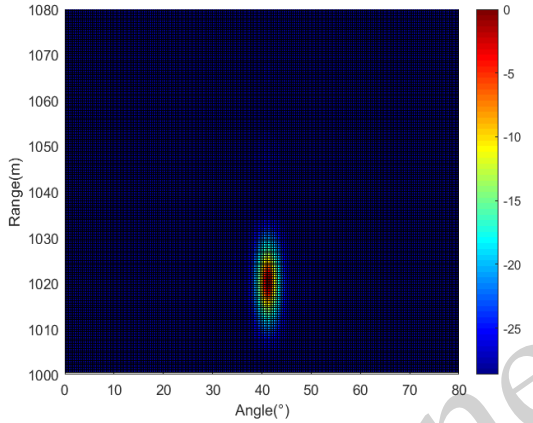

(b)

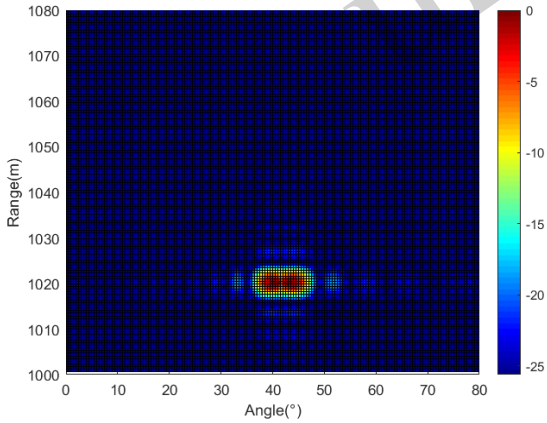

(c)

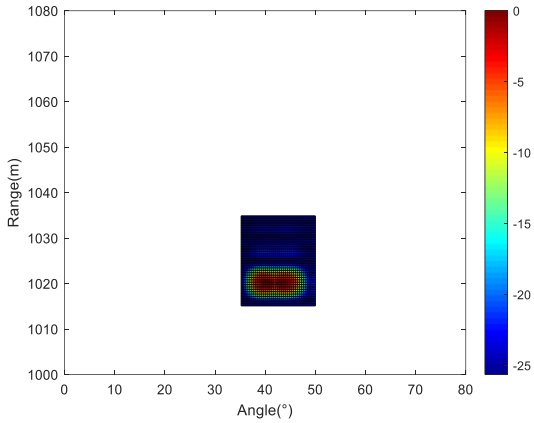

(d)

Fig. 6. Angle resolution image. ESPRIT(a). MUSIC (b). WSF (c). The proposed algorithm (d).

Figure 6 presents a spectrum plot comparing the algorithms and the proposed algorithm to reflect their resolution performance in terms of angles. It can be seen that the ESPRIT algorithm has a large error in estimating the two targets when they are at adjacent angles; the MUSIC algorithm does not identify the two targets and only detects one target, with only one spectral peak in the spectrogram, and the estimated angle is approximately the middle of the two angles. This is due to the fact that both algorithms fit the orthogonal projection matrix of the array manifold matrix to the received signal subspace rather than the noise subspace, as in MUSIC. However, overall, the proposed algorithm has fewer search iterations and is able to reduce the complexity of the algorithm while maintaining the angle resolution. The same conclusion can be seen in Figure 7 in terms of range resolution.

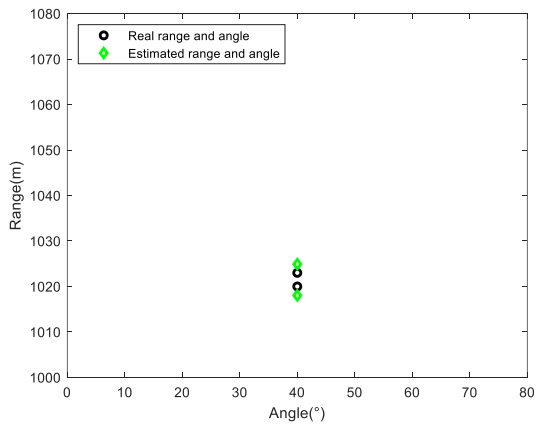

(a)

unedited

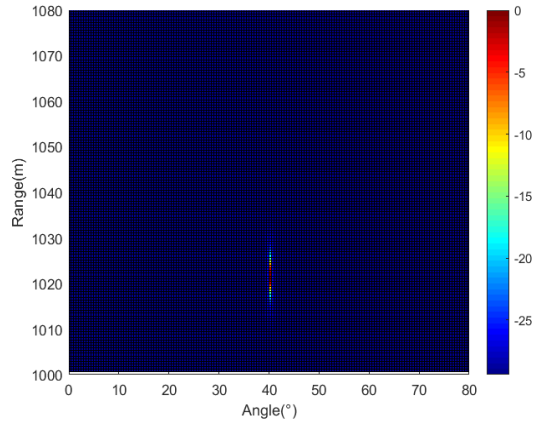

(b)

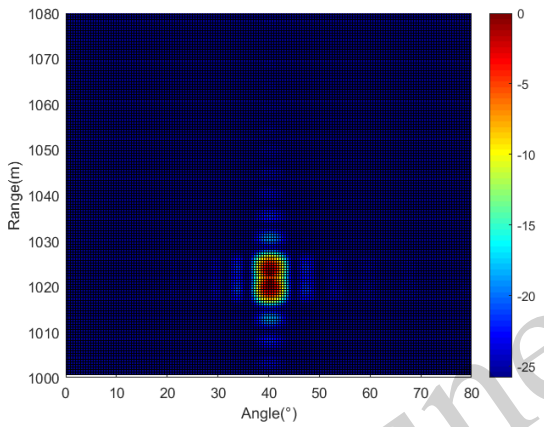

(c)

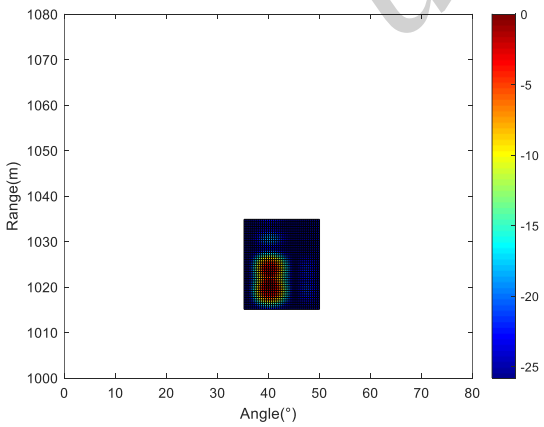

(d)

Fig. 7. Range resolution image. ESPRIT (a). MUSIC (b). WSF(c). The proposed algorithm (d).

In order to further visualize the resolution performance of the algorithm, a profile of the spectrum is plotted. The same conclusions can be drawn from Figure 8 as were drawn from Figure 6 and Figure 7. It can be seen from Figure 8 that the MUSIC algorithm, because of the two-dimensional spatial smoothing, has a lower peak parametrization from the power spectrum profile, but only forms one spectral peak, which treats the neighboring targets as one target and cannot be distinguished and accurately estimated. In contrast, the algorithm in this paper can distinguish between two targets when the targets are at the same range from each other or at the same angle, and the estimation errors for range and angle are smaller than in other algorithms.

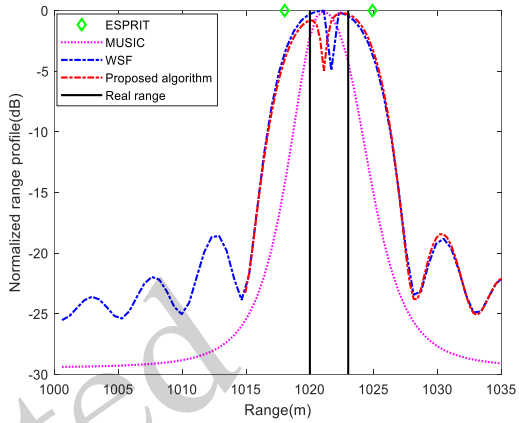

(a)

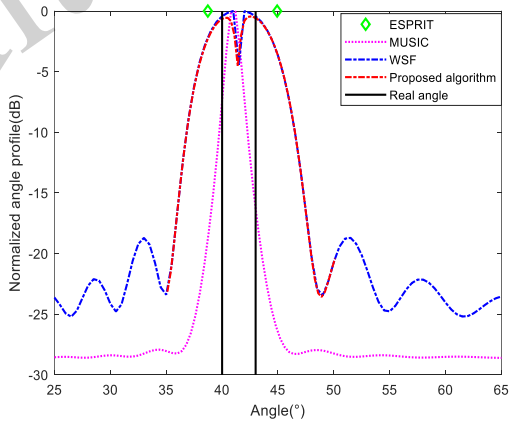

(b)

Fig. 8. Range and angle resolution cross-sections. Range (a). Angle (b).

5 Conclusion

For the angle and range estimation problem of the OTFS radar communication integration system, this paper proposes a target parameter estimation algorithm based on sparse reconstruction pre-processing. Firstly, the sparse reconstruction algorithm is used to coarse measure the angle and range of the detected target, and the search range of the range and angle is updated with the coarse measurement result as the center, after which the search grid is further subdivided to obtain accurate estimates of the

unedited

angle and range using the WSF algorithm. The theoretical analysis and simulation findings demonstrate that the proposed algorithm decreases the computational cost while ensuring the estimation accuracy and resolution capability. In our future work, we will investigate how to combine the shape, appearance, and behavioral characteristics of targets with angle and distance information to achieve more comprehensive target recognition and classification while maintaining security and privacy. This is important for applications such as autonomous driving and security surveillance.

Contributors

Zhen-kai ZHANG designed the research. Zhen-kai ZHANG, Xiao-ke SHANG and Yue XIAO performed the experiments. Xiao-ke SHANG and Yue XIAO drafted the manuscript. All authors commented on previous versions of the paper. Zhen-kai ZHANG revised the paper. All authors read and approved the final paper.

Compliance with ethics guidelines

Zhen-kai ZHANG, Xiao-ke SHANG and Yue XIAO declare that they have no conflict of interest.

References

Yan JK, Pu WQ, Zhou SH, et al., 2020. Collaborative detection and power allocation framework for target tracking in multiple radar system. Information Fusion, 55: 173-183. https://doi.org/10.1016/j.inffus.2019.08.010.

Dokhanchi SH, Mysore BS, Mishra KV, et al., 2019. A mmwave automotive joint radar-communications system. IEEE Transactions on Aerospace and Electronic Systems, 55(3): 1241-1260. https://doi.org/10.1109/taes.2019.2899797.

Zheng L, Lops M, Eldar YC, et al., 2019. Radar and communication coexistence: an over-view: a review of recent methods. IEEE Signal Processing Magazine, 36(5): 85-99. https://doi.org/10.1109/msp.2019.2907329.

Hassanien A, Amin MG, Aboutanios E, et al., 2019. Dual-function radar communication systems: a solution to the spectrum congestion problem. IEEE Signal Processing Maga-zine, 36(5): 115-126. https://doi.org/10.1109/msp.2019.2900571.

Zhang ZK, Najafabadi HE, Jin B, 2021.Transmit array resource allocation for radar and communication integration system. Measurement, 173: 108595. https://doi.org/10.1016/j.measurement.2020.108595

Sanson JB, Tomé PM, Castanheira D, et al., 2020. High-resolution delay-doppler estimation using received communication signals for ofdm radar-communication system. IEEE Transactions on Vehicular Technology, 69(11): 13112-13123. https://doi.org/10.1109/tvt.2020.3021338.

Hakobyan G, Yang B, 2017. A novel intercarrier-interference free signal processing scheme for ofdm radar. IEEE Transactions on Vehicular Technology, 67(6): 5158-5167. https://doi.org/10.1109/tvt.2017.2723868.

Li YC, Wang XD, Ding ZG, 2019. Multi-target position and velocity estimation using ofdm communication signals. IEEE Transactions on Communications, 68(2): 1160-1174. https://doi.org/10.1109/tcomm.2019.2956928.

Franken G, Nikookar H, Van GP, 2006. Doppler tolerance of ofdm-coded radar signals. 2006 European Radar Conference: IEEE, p.108-111.

R. Hadani, S. Rakib, M. Tsatsanis, et al., 2017. Orthogonal time frequency space modula-tion. 2017 IEEE Wireless Communications and Networking Conference (wcnc): IEEE, p.1-6.

Farhang A, Rezazadeh RA, Doyle LE, et al., 2017. Low complexity modem structure for ofdm-based orthogonal time frequency space modulation. IEEE Wireless Communica-tions Letters, 7(3): 344-347. https://doi.org/10.1109/lwc.2017.2776942.

Surabhi GD, Ramachandran MK, Chockalingam A., 2019. OTFS modulation with phase noise in mmWave communications[C]//2019 IEEE 89th Vehicular Technology Confer-ence (VTC2019-Spring): IEEE, p.1-5. https://doi.org/10.1109/VTCSpring.2019.8746382

Surabhi GD, Augustine RM, Chockalingam A, 2019. Peak-to-average power ratio of otfs modulation. IEEE Communications Letters, 23(6): 999-1002. https://doi.org/10.1109/lcomm.2019.2914042.

Keskin MF, Wymeersch H, Alvarado A. Radar sensing with otfs: embracing isi and ici to surpass the ambiguity barrier. 2021 IEEE International Conference on Communications Workshops (icc Workshops): IEEE, 2021: 1-6. https://doi.org/10.1109/ICCWorkshops50388.2021.9473534

Hadani R, Rakib S, Molisch A, et al., 2017. Orthogonal time frequency space (otfs) modula-tion for millimeter-wave communications systems. 2017 IEEE Mtt-s International Mi-crowave Symposium (ims): IEEE, p.681-683. https://doi.org/10.1109/MWSYM.2017.8058662

Xue JR, Wang, D, Du SY. et al., 2017. A vision-centered multi-sensor fusing approach to self-localization and obstacle perception for robotic cars. Frontiers Inf Technol Elec-tronic Eng, 18:122–138. https://doi.org/10.1631/FITEE.1601873

Patole SM, Torlak M, Wang D, et al., 2017. Automotive radars: a review of signal pro-cessing techniques. IEEE Signal Processing Magazine, 34(2): 22-35. https://doi.org/10.1109/msp.2016.2628914.

Raviteja P, Phan KT, Hong Y, et al., 2019. Orthogonal time frequency space (otfs) modula-tion based radar system. 2019 IEEE Radar Conference (radarconf): IEEE, p.1-6. https://doi.org/10.1109/RADAR.2019.8835764

Gaudio L, Kobayashi M, Caire M, et al., 2020. On the effectiveness of otfs for joint radar parameter estimation and

unedited

communication. IEEE Transactions on Wireless Communica-tions, 19(9): 5951-5965. https://doi.org/10.1109/twc.2020.2998583.

Gaudio L, Kobayashi M, Caire M, et al., 2020. Joint radar target detection and parameter estimation with mimo otfs. 2020 IEEE Radar Conference (radarconf20): IEEE, p.1-6. https://doi.org/10.1109/RadarConf2043947.2020.9266546

Liu CW, Liu SH, Mao ZH, et al., 2021. Low-complexity parameter learning for otfs modula-tion based automotive radar. Icassp 2021-2021 IEEE International Conference on Acoustics, Speech and Signal Processing (icassp): IEEE, p.8208-8212. https://doi.org/10.1109/ICASSP39728.2021.9414107

Li SY, Yuan WJ, Liu C, et al., 2022.A novel isac transmission framework based on spatial-ly-spread orthogonal time frequency space modulation. IEEE Journal on Selected Areas in Communications, 40(6): 1854-1872. https://doi.org/10.1109/jsac.2022.3155538.

Shi WT, Zhang QF, He CB, et al., 2019. Taylor expansion MUSIC method for joint DOD and DOA estimation in a bistatic MIMO array. Front Inform Technol Electron Eng, 20: 842–848. https://doi.org/10.1631/FITEE.1700657

Wang XJ, Zhang ZK, Esmaeili NH, 2021. Joint range and velocity estimation for integration of radar and communication based on multi‐symbol ofdm radar pulses. IET Radar, So-nar & Navigation, 15(5): 533-545. https://doi.org/10.1049/rsn2.12071.

Zhang FQ, Zhang ZH, Yu WX, et al., 2020. Joint range and velocity estimation with intrap-ulse and intersubcarrier doppler effects for ofdm-based radcom systems. IEEE Transac-tions on Signal Processing, 68: 662-675. https://doi.org/10.1109/tsp.2020.2965820.

Zheng L, Wang XD, 2017. Super-resolution delay-doppler estimation for ofdm passive radar. IEEE Transactions on Signal Processing, 65(9): 2197-2210. https://doi.org/10.1109/tsp.2017.2659650.

Rahman ML, Zhang JA, Huang X, et al., 2020. Joint communication and radar sensing in 5g mobile network by compressive sensing. IET Communications, 14(22): 3977-3988. https://doi.org/10.1049/iet-com.2020.0384.

Ottersten B, Viberg M, Kailath T, 1992. Analysis of subspace fitting and ml techniques for parameter estimation from sensor array data. IEEE Transactions on Signal Processing, 40(3): 590-600. https://doi.org/10.1109/78.120802.

Keskin M F, Wymeersch H, et al., 2021. Radar sensing with OTFS: Embracing ISI and ICI to surpass the ambiguity barrier. 2021 IEEE International Conference on Communica-tions Workshops (ICC Workshops): IEEE, p.1-6. https://doi.org/10.1109/ICCWorkshops50388.2021.9473534

Ottersten B, Viberg M, Stoica P, et al., 1993. Exact and Large Sample Maximum Likelihood Techniques for Parameter Estimation and Detection in Array Processing. Radar Array Processing, 25: 99-151.

unedited